Journal of Hydrology 460–461 (2012) 40–51

Contents lists available at SciVerse ScienceDirect

Journal of Hydrology

journal homepage: www.elsevier.com/locate/jhydrol

Using subsurface temperatures to derive the spatial extent of the land use change effect

Luminda Niroshana Gunawardhana *, So Kazama

Graduate School of Engineering, Tohoku University, Aoba 6-6-06, Sendai 980-8579, Japan

ARTICLE INFO

Article history:
Received 16 January 2012
Received in revised form 29 May 2012
Accepted 15 June 2012
Available online 4 July 2012
This manuscript was handled by Corrado Corradini, Editor-in-Chief, with the assistance of Dr. M. Laba, Associate Editor

Keywords:
Urban heat island
Aquifer temperature
Spatial extent
NDVI
Japan

SUMMARY

The urban heat island (UHI) effect has traditionally been determined using ambient air temperatures or land surface temperatures derived from satellite observations. In this study, we used the subsurface temperature anomaly as an indicator in describing a relationship between land use characteristics and aquifer temperature changes in the shallow subsurface layers of three rapidly developing urban settings: the Kanto, Sendai and Chikushi plains in Japan. Information on land cover was derived from Landsat Enhanced Thematic Mapper Plus (ETM+) images acquired between 1999 and 2001. The supervised classification technique along with the Normalized Difference Vegetation Index (NDVI) was used to specify the urban degree for grid cells covering observation wells. Preliminary analysis of groundwater levels in different well locations revealed that vertical groundwater recharge is predominant in all study areas. A numerical model for subsurface heat transport employed with different groundwater recharge/discharge and ground surface warming rates indicated that ground surface warming has a significant effect on aquifer temperatures in shallow subsurface layers. The results show that the magnitude of aquifer temperature change is positively correlated with the degree of impervious area derived from the NDVI values (i.e., negatively correlated with the NDVI value with 0.5–0.7 °C warming for a 0.12 NDVI difference at a 20-m depth). The relationship between aquifer temperature changes and grid-averaged NDVI values was strongest at an area of approximately 99,225 m^2 (roughly equal to an area with a 175-m radius) and determination coefficient equal to 0.91 for the Kanto plain. As the average area is further increased, the relationship between the two variables gradually became weaker. According to results verified for the Sendai and Chikushi plains, the same relationship was achieved for areas no larger than 175 (±15) m radius and a determination coefficient of 0.81, which is suggested as the operational spatial scale to determine the UHI effect on subsurface thermal regimes. As the necessity for adaptation measures to cope with urban thermal pollution is increasingly understood, the lateral extent of subsurface heat flow found in this study may be useful in urban planning and habitat restoration programs.

1. Introduction

The dramatic warming trend in urban areas in the 20th century cannot be attributed to global climate change alone. For example, meteorological records have revealed that the surface air temperature warming rate was as high as 3.3 °C/century from 1950 to 2005 in the center of Bangkok, Thailand (Taniguchi, 2006), 2.0 °C/century from 1921 to 2010 in Tokyo and 2.2 °C/century from 1926 to 2010 in Sendai, Japan. According to an analysis performed by Hansen and Lebedeff (1987), the magnitude of global averaged rise in surface air temperatures from 1880 to 1985 was approximately 0.5 °C/century. Huang et al. (2000) used temperatures from 616 boreholes to reconstruct global temperature trends over the past 500 years at a global scale and estimated a 0.5 °C/century surface warming trend in the 20th century. Therefore, the rapid warming trends in urban areas are due not only to the effects of global climate change, but also to increases of macro-scale air and surface temperatures caused by the urbanization effect, which is referred to as the urban heat island (UHI).

Diurnal and seasonal changes in surface air temperature are strongly correlated with shallow subsurface temperature variations (Gunawardhana and Kazama, 2009). Therefore, the UHI effect has significantly influences aquifer temperatures (Ferguson and Woodbury, 2004), which may be more persistent and profound than the impact on surface air temperatures (Huang et al., 2009). Ecologically, groundwater discharge during summer months can be essential in maintaining desirable thermal conditions for aquatic species because groundwater temperature is less variable in seasonal scale and cooler than the stream water temperature (Drake et al., 2010). Therefore, aquifer warming due to UHI is of prime importance to assess the environmental conditions suitable for aquatic ecosystems.

* Corresponding author. Tel.: +81 90 1397 3047; fax: +81 22 295 7458.
E-mail address: luminda@kaigan.civil.tohoku.ac.jp (L.N. Gunawardhana).

0022-1694/$ - see front matter © 2012 Elsevier B.V. All rights reserved.
http://dx.doi.org/10.1016/j.jhydrol.2012.06.042

Due to the much higher heat capacity and low thermal diffusivity of aquifers relative to air, changes on the ground surface over a 100 years can be detected within depths of 100 m (Harris and Chapman, 1997; Taniguchi et al., 1999). Conversely, because of the rapid convective heat transport that occurs in air, atmospheric temperature changes caused by the UHI effect diffuse efficiently into surrounding areas by attenuating urban warmth at the origin (Arnfield, 2003). Therefore, even if the magnitude of the surface air temperature change agrees with the ground surface temperature change at a large scale (Pollack et al., 1998; Huang et al., 2000), surface air temperature records alone may not represent the total impact of urban heat island effects on the thermal regime of an aquifer (Huang et al., 2009).

Many studies use air temperature data gathered by automobile traverses or recorded by meteorological stations to determine the UHI intensity, which are further supported by records such as population density and wind speed (Oke, 1973; Sakakibara and Owa, 2005; Kataoka et al., 2009). With the advancement of remote sensing techniques, recent studies have used vegetation index and surface temperature derived from the satellite data to estimate the UHI intensity (Gallo et al., 1993; Weng et al., 2004; Hung et al., 2006). However, no study has taken advantage of the potential for aquifer temperatures to determine the spatial scale of subsurface warming. This study presents the use of borehole temperatures and a remote sensing-based, land-use classification technique in three urban settings (the Kanto, Sendai and Chikushi plains in Japan) to determine an operational spatial scale for subsurface warming. The paper begins with an analysis of multidimensional groundwater flow to understand the effect of horizontal groundwater flows on the temperature distribution in shallow subsurface layers, followed by a development of a numerical model to show the influence of ground surface warming for temperature variations in shallow subsurface layers, and finally, we develop and test a relationship between land use characteristics and aquifer warming in the shallow subsurface layers to introduce a new operational spatial scale to determine the UHI effect on subsurface thermal regimes. As many attempts are currently being made to mitigate the thermal impacts of urban settings, the findings from this study will be useful for habitat restoration programs.

2. Study area and data collection

The three selected study areas are among the cities that have undergone rapid urbanization during the 20th century in Japan. In response to excessive groundwater extraction and subsequent land subsidence, the Japanese government imposed regulations on groundwater pumping for industrial use in 1956 and for urban use in 1963.

2.1. Kanto plain

The Kanto plain covers an area over 16,840 km^2 and is surrounded by the Tanzawa, Kanto, Asio and Yamizo mountain ranges. Many tributaries of the Tone, Watarase, Kinu, Kokai, Naka, Arakawa, Tama and Sugami Rivers emerge from the peripheral mountain ranges in this region and flow through its low land areas, including the Tokyo city area, ending in Tokyo Bay (Fig. 1). The geology of the Kanto plain is primarily alluvial and presents three sedimentary layers, which are identified as the Shimousa group at the top (100–400 m from the ground surface to the bottom depth), the Kazusa group in the middle (500–1500 m from the ground surface to the bottom depth) and the Miura group at the bottom, which forms a rich aquifer more than 3000 m in thickness (Miyakoshi et al., 2003). Regarding the shallow subsurface layers, the upland area of the plain is mainly covered by the Kanto loam, a relatively permeable volcanic ash that is 5–10 m in thickness and underlain by a sand and gravel layer. The lowland area is formed by an alluvial layer that is 10–40 m in thickness and beneath the silt, sand and gravel layers (Suzuki, 1996).

In this study, 43 of the 88 temperature–depth profiles presented in the Water Environmental Map No. 3 (Miyakoshi and Uchida, 2001; AIST, 2005) were used for the Kanto plain (Fig. 2a). Many temperature–depth profiles were excluded because of lack of observations at deeper aquifer depths and abrupt changes that attributed to the meso-scale groundwater flow and geological variations. The depth of the observation wells extended up to 600 m from the ground surface. All of the above measurements were taken from October 14, 1999 to November 20, 2000 using a thermistor thermometer with an accuracy of 0.01 °C. Moreover, groundwater levels from three observation wells that were averaged daily from January 1, 2005 to December 31, 2005 were obtained from the Water Information System (WIS), Ministry of Land, Infrastructure and Transport (MLIT) in Japan.

2.2. Sendai plain

The Sendai plain, located in northeastern Japan, is formed by an approximately 400 km^2 lowland area in the vicinity of the Zao and Funagata mountains. The Nanakita, Natori and Abukuma Rivers commence in the mountain region and flow through urban Sendai toward the Pacific Ocean. The geology of the Sendai plain is alluvial and contains a clay layer (5–10 m in thickness) above a silt and sand layer (10–20 m in thickness). The depth of the aquifer ranges from 20 to 80 m, which is substantially shallower than that of the aquifer of the Kanto plain (additional details provided in Uchida and Hayashi, 2005).

For the Sendai plain, the aquifer temperatures from nine observation wells presented in the Water Environmental Map No. 1 (AIST, 2004) were obtained (Fig. 2b). Three of these observation points include three nested wells in each directed to different aquifer depths and different screen intervals. The monthly averaged water level records (daily water level records averaged over each month) for the past 20 years and 1-h water level records from April 1, 2004 to July 31, 2007 were collected for the majority of these well points.

2.3. Chikushi plain

The Chikushi plain, located in the Kyushu Island, is formed by a lowland area surrounded by the Sefuri, Minou, Chikushi and Kishima mountains. Four major rivers (the Yabe, Chikugo, Kase and Rokkaku) flow through the plain and end in the Ariake Bay. The aquifer of the Chikushi plain is alluvial and extends to a maximum depth of approximately 600 m. The shallow subsurface layer is composed of clay with a maximum thickness of 30 m that is underlain by sand gravels (Fujii et al., 2007).

For the Chikushi plain, we obtained aquifer temperatures for 11 of the 28 observation wells presented in the Water Environmental Map No. 5 (AIST, 2008) (Fig. 2c). Moreover, the daily averaged groundwater levels over a 1-year period in 2005 from 10 observation wells were obtained from the WIS.

3. Methodology

In principle, heat in subsurface layers is distributed by conduction and advection caused by recharging or discharging water flows. Generally, aquifer temperatures are higher than the annual average ground surface temperature resulting from the upward heat flow from the earth's interior. In the absence of a strong groundwater flow, this phenomenon produces an approximately

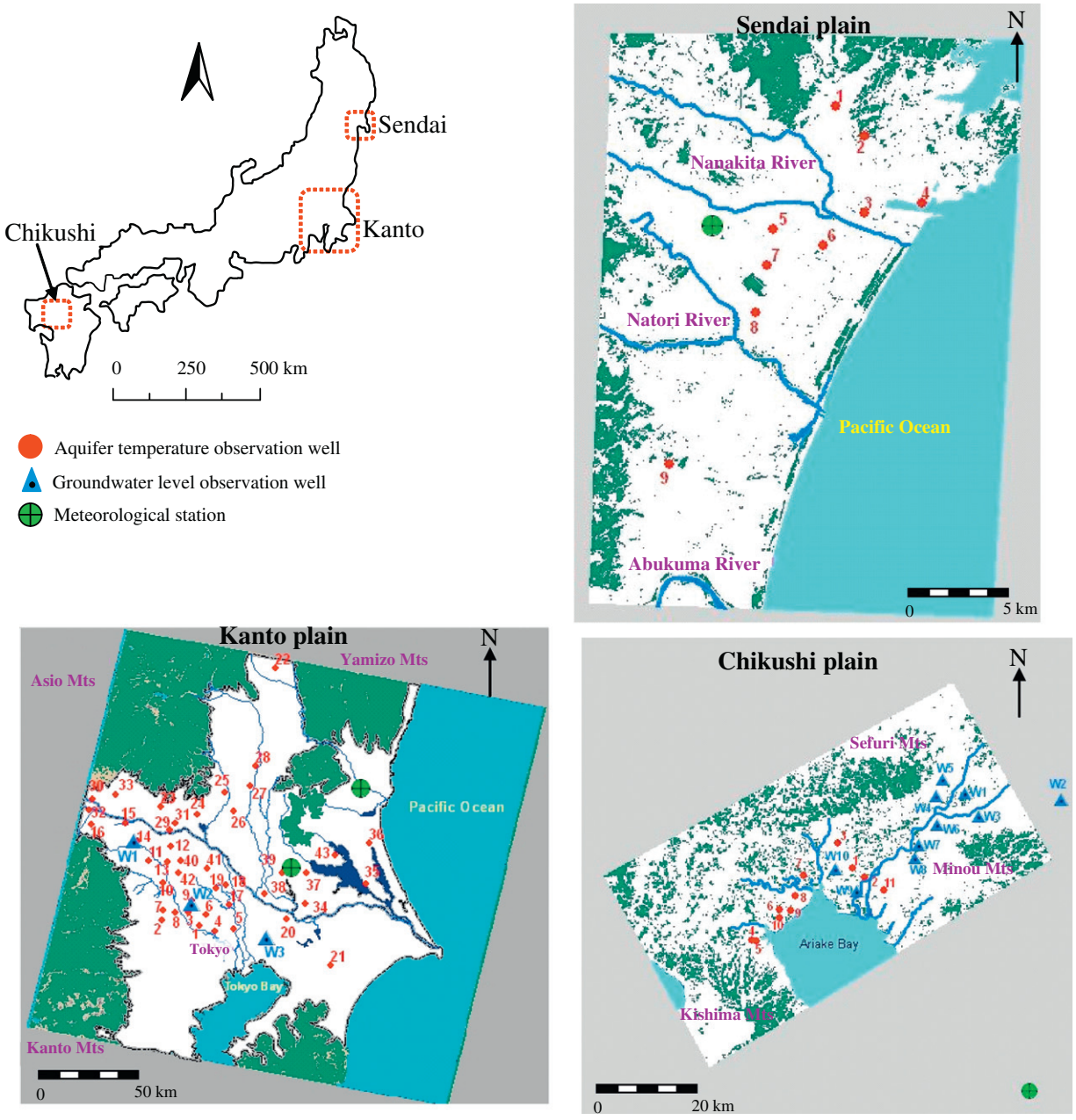

Fig. 1. The three study areas and locations of the aquifer temperature and groundwater level observation wells.

linear temperature–depth (T–D) profile within homogeneous depth intervals (e.g., 5 mm/year reported by Majorowicz et al. (2006)). When the vertical groundwater flow is comparatively large (e.g., 200 mm/year, as reported in Gunawardhana et al., 2011), the curvature of the temperature–depth profiles changes accordingly. In the presence of a horizontal groundwater flow, the temperature–depth profiles do not exhibit increasing temperature with increasing depth; instead, over a specific depth range, temperatures may decrease or remain constant with increasing depth (e.g., Figs. 1 and 2 in Ziagos and Blackwell, 1986). This phenomenon of an inverted temperature–depth profile was observed in our study areas at deep aquifer depths (e.g., W19 in Fig. 2a). Therefore, to understand the effect of horizontal groundwater flows on the temperature distribution in shallow subsurface layers, a cross-correlation analysis of water level records in different well locations was performed.

3.1. Analysis of multidimensional groundwater flow

The mathematical representation of a simple one-dimensional groundwater flow in a homogeneous aquifer can be written as in following equation:

$$K\frac{\partial^2 h}{\partial x^2} = S_C\frac{\partial h}{\partial t} \tag{1}$$

where K is the aquifer hydraulic conductivity; h is the water head; S_C is the aquifer storage coefficient; and t is time. When the following initial and boundary conditions are applied

$$h_{t=0} = 0, \quad \text{for} \quad 0 < x < \infty \tag{2}$$

$$h_{x=0} = h_0, \quad \text{for} \quad t > 0 \tag{3}$$

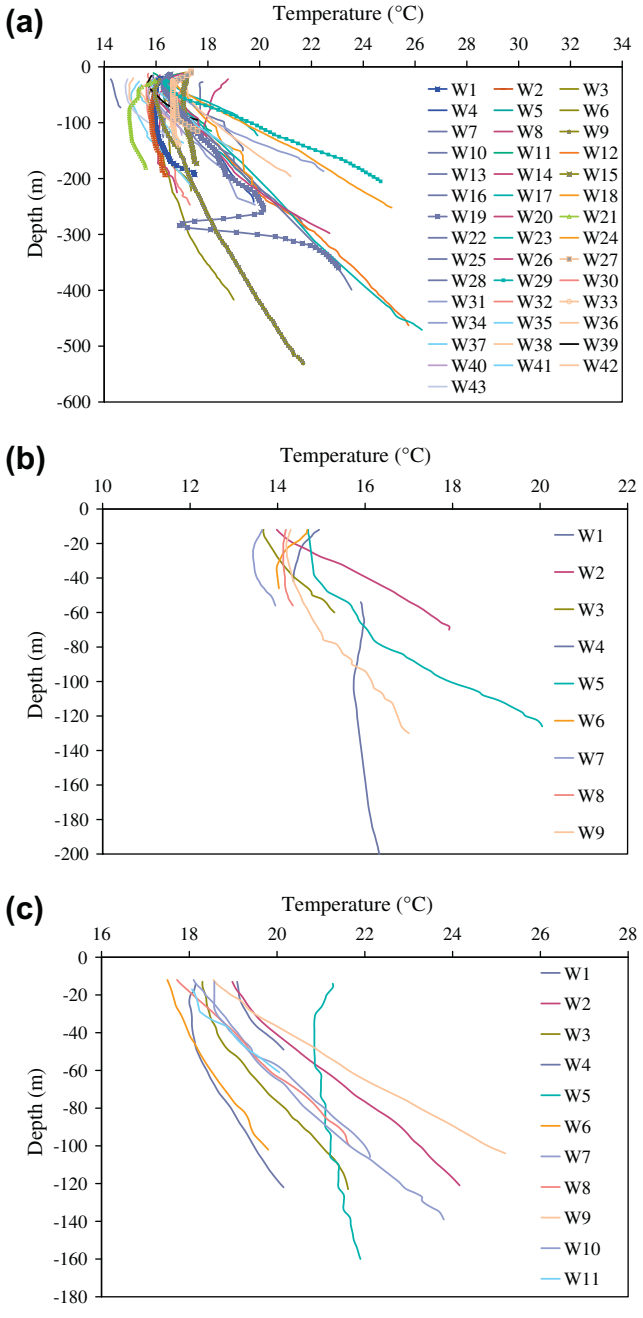

Fig. 2. The temperature–depth profiles used for the analysis. (a) Kanto plain, (b) Sendai plain and (c) Chikushi plain.

an analytical solution for Eq. (1) can be written as Eq. (4).

$$h(x,t) = h_0 \mathrm{erfc}\left(\sqrt{S_C/2K}\frac{x}{\sqrt{t}}\right) \tag{4}$$

When a complementary error function is used as the aquifer response, the variation in the water level at one point located in the path of water flow ($H(x,t)$) can be expressed with a certain time lag as a convolution of the water recharge ($R(t)$) at another point and the aquifer response function (Chen et al., 2002).

$$H(x,t) = \int_0^t R(t)g(x,\tau - t)dt \tag{5}$$

where

$$g(x,t) = \mathrm{erfc}\left(\sqrt{S_C/2K}\frac{x}{\sqrt{t}}\right) \tag{6}$$

The time lag can be determined by cross-correlation analysis of water level fluctuations at the recharge point and the response point. Thus, an artificial groundwater recharge time series was generated using the observed groundwater level data in well 6 (the Sendai plain). The daily average groundwater levels from April 1, 2004 to July 31, 2007 were filtered with a moving average technique to produce a low-pass recharge time series. A system response function with various aquifer properties was then convolved with the generated recharge time series to obtain the water level fluctuation at a 50-km distance point from the recharge point. A cross-correlation analysis was finally performed with the artificially generated recharge water levels and the simulated water level variations at a 50-km distance point. The resulting time delay was then compared with time delays estimated from a cross-correlation analysis performed with the observed water levels in the shallow subsurface layers (10–40 m) at different well points.

In addition to the effect of horizontal groundwater flow, changes in ground surface temperatures attributed to man-made modifications (e.g. UHI effect) gradually penetrate subsurface layers and, consequently, alter the shape of the temperature–depth profile. It is, therefore, important to understand the significance of the various heat transport processes when distributing temperatures in shallow subsurface layers. Accordingly, a numerical model was developed and an observed temperature–depth profile for the Kanto plain was used for comparison with the numerically simulated results.

3.2. Simulation of the temperature distribution in subsurface layers

The VS2DH numerical code (Healy and Ronan, 1996) used in this study can simulate heat transport under unsteady, non-uniform water movement and with variable boundary conditions (Su et al., 2004; Essaid et al., 2008; Duque et al., 2010). The governing equation for subsurface temperature distribution can be written as follows:

$$\partial/\partial t[\theta C_W + (1-\phi)C_S]T = \nabla \cdot K_T(\theta)\nabla T + \nabla \cdot \theta C_W D_H \nabla T - \nabla \theta C_W \upsilon T + qC_W T^* \tag{7}$$

where t is time in s; θ is the volumetric moisture content; C_W is the heat capacity of water in J/m^3°C; ϕ is porosity; C_S is the heat capacity of the dry soil in J/m^3°C; T is temperature in °C; K_T is the water and solid matrix thermal conductivity in W/m °C; D_H is the hydrodynamic dispersion tensor in m^2/s; υ is water velocity in m/sec; q is the rate of the fluid source in s^{-1}; and T^* is the temperature of the fluid source in °C.

The domain was modeled using 230 rows in which grid spacing varied from 0.1 m at the surface to 1 m in depth; the total domain depth was 200 m. All of the parameter values were based on data from the Geological Survey of Japan and previous studies (Table 1). For the initial and boundary conditions, the temperatures at the bottom and top of the porous medium were assigned based on the undisturbed linear portion of the T–D profile. The temperature at the bottom of the model was treated as a constant throughout the simulation. According to meteorological records from 1891,

Table 1
Parameter values used for the numerical simulation.

Parameter	Value
Hydraulic conductivity (m/s)	1×10^{-6}–1×10^{-8}
Porosity	0.3–0.2
Residual moisture content	0.02
Heat capacity of dry soil (J/m^3/°C)	2.08–2.18 $\times 10^6$
Heat capacity of water (J/m^3/°C)	4.18 $\times 10^6$
Thermal conductivity of soil (W/m^3/°C)	1.3–1.6

the surface air temperature in the three regions showed no significant warming trend until the mid-20th century, but began to warm rapidly in 1947 with increased rates of 2.9, 1.9 and 1.7 °C/100 years observed in Chikushi, Sendai and Kanto, respectively (Fig. 3a). Therefore, 1947 was selected as the start time for the model to determine the aquifer temperature change attributed to ground surface temperature variations over 53 years (aquifer temperatures were measured in 2000). However, precipitation in these areas has shown no significant trend from 1891 to the present (Fig. 3b). Therefore, the advective effect of groundwater recharge/discharge must have altered the temperature–depth profile over a long time period. For this reason, the numerical model was run for over 100 years to determine the aquifer temperature change caused by the advective effect of groundwater (approximately two times larger than the model run with ground surface temperature variations).

Because the actual ground surface histories were unknown, the surface air temperature (Fig. 3a) was used as a proxy and filtered using a 5-year moving average (Majorowicz et al., 2006). The estimated ground surface temperatures showed less variation than the surface air temperatures. However, long-term comparisons followed a trend that was similar to that observed for surface air temperature changes (Huang et al., 2000). The ground surface temperatures from 1947 to 2000 were first corrected to zero trends. The deviations in the estimated ground surface temperature from 1947 to 2000 averages were then added to the estimated initial ground surface temperature to incorporate the ground surface temperature change over time. To incorporate the different warming rates attributed to different levels of urbanization, various warming rates (e.g., 1–5 °C/100 years) were then added to the ground surface temperature series.

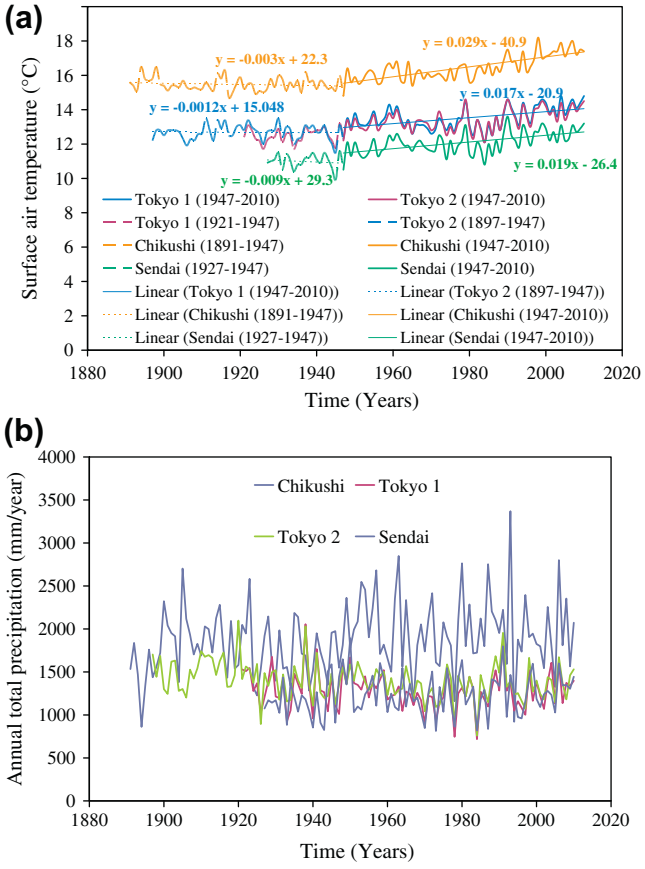

Fig. 3. The meteorological observations in the three study areas. (a) Surface air temperature and (b) precipitation.

3.3. Normalized vegetation index and land cover classification

The advancement of satellite remote sensing technology has made it possible to study land use changes at fine resolutions and broad spatial scales. Landsat 7 Enhanced Thematic Mapper Plus (ETM+) images with a high spatial resolution (30 m for bands 1–7 and 15 m for the panchromatic band) acquired on October 21, 1999 for the Kanto plain, October 26, 2001 for the Sendai plain and October 01, 2000 for the Chikushi plain were obtained through the USGS Earth Resource Observation Systems Data Center. These images have been corrected for the systematic radiometric and geometric accuracy by incorporating ground control points while employing a Digital Elevation Model (DEM) for topographic accuracy. To analyze urban land cover/vegetation cover characteristics, the Normalized Difference Vegetation Index (NDVI) (Eq. (8)), one of the most commonly adopted urban–rural landscape classification techniques, was employed (Epperson and Davis, 1995; Weng et al., 2004; Hung et al., 2006). The Panchromatic band at a 15-m spatial resolution was used with a pan-sharpening technique to obtain a higher resolution classification map.

$$\mathrm{NDVI} = \frac{[\mathrm{Band\ 4} - \mathrm{Band\ 3}]}{[\mathrm{Band\ 4} + \mathrm{Band\ 3}]} \tag{8}$$

The use of gridded data with a spatial average is a common technique for UHI studies (e.g., Kataoka et al., 2009; Weng et al., 2004). In this study, the NDVI values corresponding to grid values in the land use map were averaged around each observation well for various spatial scales (e.g., 3 pixels × 3 pixels produced a 45 m × 45 m average area) and matched with the aquifer temperature changes in the shallow subsurface layers. The magnitude of aquifer warming was estimated at three comparatively deeper depths (20, 30 and 40 m) to avoid the effect of seasonal surface air temperature changes (Gunawardhana and Kazama, 2009). Out of the 63 temperature–depth profiles in the three study areas, there were 11 with an absence of observations at approximately 20-m depths and/or without a smooth transient perturbation profile. For these cases, numerical models were developed following the method explained in Section 3.2 and matched with the observed temperature–depth profile at each well location. The magnitude of aquifer warming was calculated as the difference between the simulated profile and the general geothermal gradient for particular depths.

4. Results

From the three stages of the methodology, the first stage was devoted to understand the effect of horizontal groundwater flows on the temperature distribution in shallow subsurface layers. The results described in the following section will demonstrate the lateral heat flow in our study areas which, if strong, could potentially create a bias on temperature anomalies resulting from UHI.

4.1. Results of multidimensional groundwater and heat flow analysis

According to Fig. 4a, the simulations show clear time lags (35, 84 and 95 days for $S_C/K = 5 \times 10^{-5}$, $=5 \times 10^{-6}$ and $=5 \times 10^{-7}$, respectively) when reaching the maximum correlation between the two artificially-generated time series. Fig. 4b and c shows the results of a cross-correlation analysis performed with the observed water levels in the shallow subsurface layers at different well points in the Kanto and Chikushi plains. High cross-correlations (0.92–0.53) are seen with no time delay for the water level fluctuations between different observation wells in both plains. A similar phenomenon is also seen at the well points in the Sendai plain (Gunawardhana & Kazama, 2012). If there is a dominant horizontal

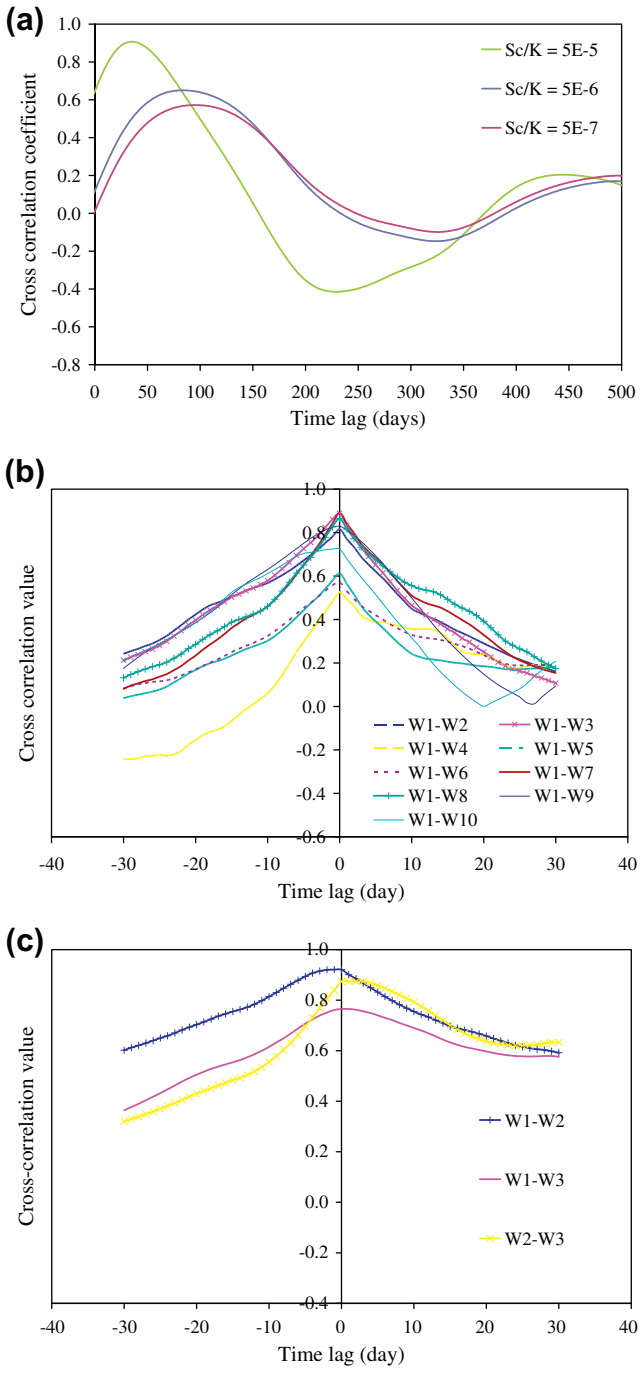

Fig. 4. Cross-correlation analysis of the water level time series at different well locations. (a) Artificially-generated time series, (b) Chikushi plain and (c) Kanto plain.

water flow toward the sea and considering the distance between W1 and W3 in the Kanto plain (Fig. 1), we would expect a maximum correlation in water level fluctuations to occur with a delay of approximately 50 days. With no apparent time delays, we therefore conclude that vertical groundwater flow is the dominant advective heat transport mode at shallow depths compared to horizontal water flow in the selected study areas.

In the second stage of this study, we developed a numerical heat transport model to incorporate ground surface warming attributed to UHI and the vertical groundwater flow effects on the temperature distribution at shallow subsurface layers. The result presented in the next section will compare the significance of each process for changing shallow aquifer thermal regimes.

4.2. Ground surface warming effect on shallow aquifer thermal regimes

Fig. 5a depicts the aquifer temperature change for different recharge/discharge rates, whereas the ground surface warming rate = 0. According to simulations 1–3, the temperature–depth profiles are concave with respect to recharge water flow and convex with respect to discharge water flow. This is because the aquifer temperature is higher at deeper depths than at shallow aquifer depths. Therefore, recharge flux brings cold water down to deep aquifer depths, and an upward flux transports warm water toward the ground surface. This result elevated the aquifer temperature in discharge areas and lowered the aquifer temperature in recharge areas compared to the aquifer temperature produced by the general geothermal gradient. Simulation 4 shows the temperature–depth profile for a 100-year simulation (approximately two times longer than simulations 1–3). According to all four simulations, neither the infiltrating recharge flux nor the discharge water flow caused significant temperature changes in the shallow subsurface layers within the depths of interest (1–20 m in general). This is because the geothermal gradient is driven by the very large temperature difference between the earth's interior and the ground surface (e.g., 2 °C/100 m in Fig. 5). Thus, a small change caused by the downward/upward movement of cool/warm water flow may not significantly alter the natural geothermal gradient. Fig. 5b shows the aquifer temperature change for different ground surface warming rates, while the recharge rate is held constant

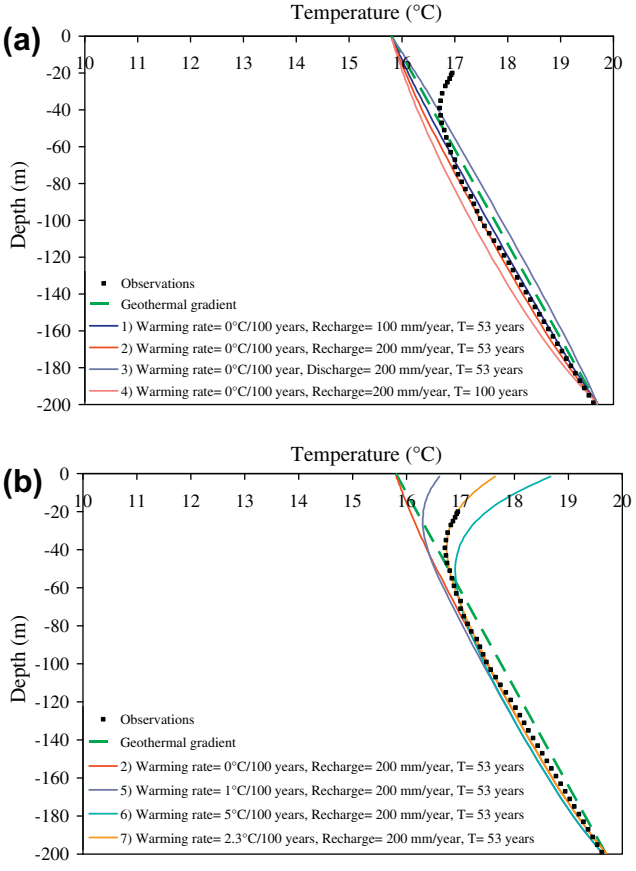

Fig. 5. Numerically simulated temperature–depth profiles for different recharge/discharge and ground surface warming rates.

(the best-fit recharge rate for the observed temperature profile in Fig. 5b). When comparing simulations 5–7 (Fig. 5b) with simulations 1–4 (Fig. 5a), ground surface warming is more profound and significant for temperature variations in shallow subsurface layers. Moreover, the estimated ground surface warming rate in Fig. 5b (2.3 °C/100 years) is comparatively larger than the surface air temperature warming rate in the Kanto plain (1.7 °C/100 years), which confirms the difference in the urban heat island effect between the surface and subsurface environments.

Numerous studies have found a direct impact on subsurface thermal regimes following land use change (Bense and Beltrami, 2007; Ferguson and Beltrami, 2006). This occurs for a number of reasons: changes in albedo; changes in evapotranspiration; and changes in the thermal insulation provided by vegetation and surface soil layers. Subsequent impacts may cause significant changes in subsurface temperatures reaching beyond the extent of the affected area at the surface (Ferguson and Beltrami, 2006). Accordingly, following section explains a relationship that was developed between the spatially averaged urban degree (in terms of the NDVI value) and the change in aquifer temperature from its natural state.

4.3. Relationships between land use characteristics and aquifer warming

The supervised classification method was used to classify each study area into four broad land cover classes corresponding to water, impervious surfaces, agriculture and forest. The overall classification accuracies for the land cover categories were 82%, 87% and 91% for the Kanto, Chikushi and Sendai plains, respectively. The impervious surface category was further divided into 10 classes to show the degree of imperviousness from high-density urban settings to low-density residential areas. Fig. 6 shows the classified land use map for the Kanto plain. Due to the high reflectance of water and snow, the NDVI values for these classes range from −1 to −0.09. The NDVI values for typical impervious areas range from −0.09 for high-density urban settings to 0.03 for low-density residential areas. In areas with vegetation, the NDVI is normally greater than 0.03 for vacant spaces with bare soil, seasonal vegetation and agricultural classes. Higher NDVI values are associated with high-density green areas that commonly occur in mountain forests (Epperson and Davis, 1995).

Fig. 7 shows the relationships developed between the aquifer temperature change at a 20-m depth and the spatially averaged NDVI values for various spatial scales in the Kanto plain. The magnitude of the aquifer temperature change shows strong negative correlations with the NDVI value (i.e., positively correlated with the degree of impervious area). The land use characteristic of the grid box containing the observation well alone is not capable of producing a strong relationship for aquifer temperature changes (Fig. 7a). This is due to the heat loss from high-density urban areas to low-density urban areas that extend laterally for a certain distance. For example, Ferguson and Woodbury (2004) found that the heat loss from two buildings that are 50 m from each other was capable of increasing the aquifer temperatures between the two buildings by 4–5 °C after 100 years. When different scales were examined, a spatial average of 99,225 m^2 (Fig. 7b), which is approximately equals to a circle with a 175-m radius, produced the best-fit relationship with a determination coefficient equal to 0.91 (Fig. 7d). As the average area is increased further, the relationship between the two variables gradually grows weaker (Fig. 7c and d). Weng et al. (2004) investigated the relationship between land surface temperature derived from remote sensing data and the NDVI value and found that the resolution of 120-m provides the strongest correlation between the two variables. In this study, the determination coefficient between the two variables was found to be 0.8 at a 120-m spatial resolution, showing a reasonable correspondence with the results of Weng et al. (2004).

The same relationship was tested for the aquifer temperature change at 30 m and 40 m. In both cases, the strongest relationship was found for a spatial average of 99,225 m^2. However, the determination coefficient decreases slightly as the impact assessment depth increases (Fig. 8). There are two potential causes of this behavior. First, the strength of the downward penetrating temperature anomaly attributed to ground surface temperature variations becomes weaker at increasing depths. For example, the extent of aquifer warming is as high as 0.7 °C for a 0.12 NDVI difference at a 20-m depth (Fig. 7b), whereas the amount of warming is as low as 0.3 °C for the same NDVI difference at a 40-m depth (Fig. 8b). Therefore, after certain depths that present more elevated aquifer temperatures above background temperatures, the temperature–depth profile simply follows the general geothermal gradient. Second, regional groundwater flow generally occurs at greater depths in aquifers exhibiting an inverted temperature–depth profile according to the magnitude of the flow.

The classified land use maps and temperature–depth profiles in the other two study areas were used to verify the accuracy of the relationship developed for the Kanto plain. Fig. 9 depicts the relationship developed between the spatially averaged NDVI values and the aquifer temperature change at a 20-m depth in the

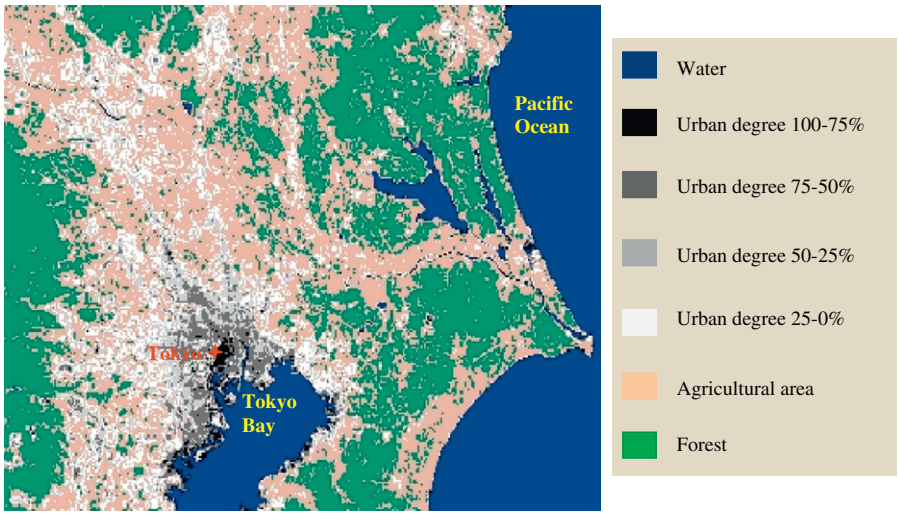

Fig. 6. The classified land use map for the Kanto plain.

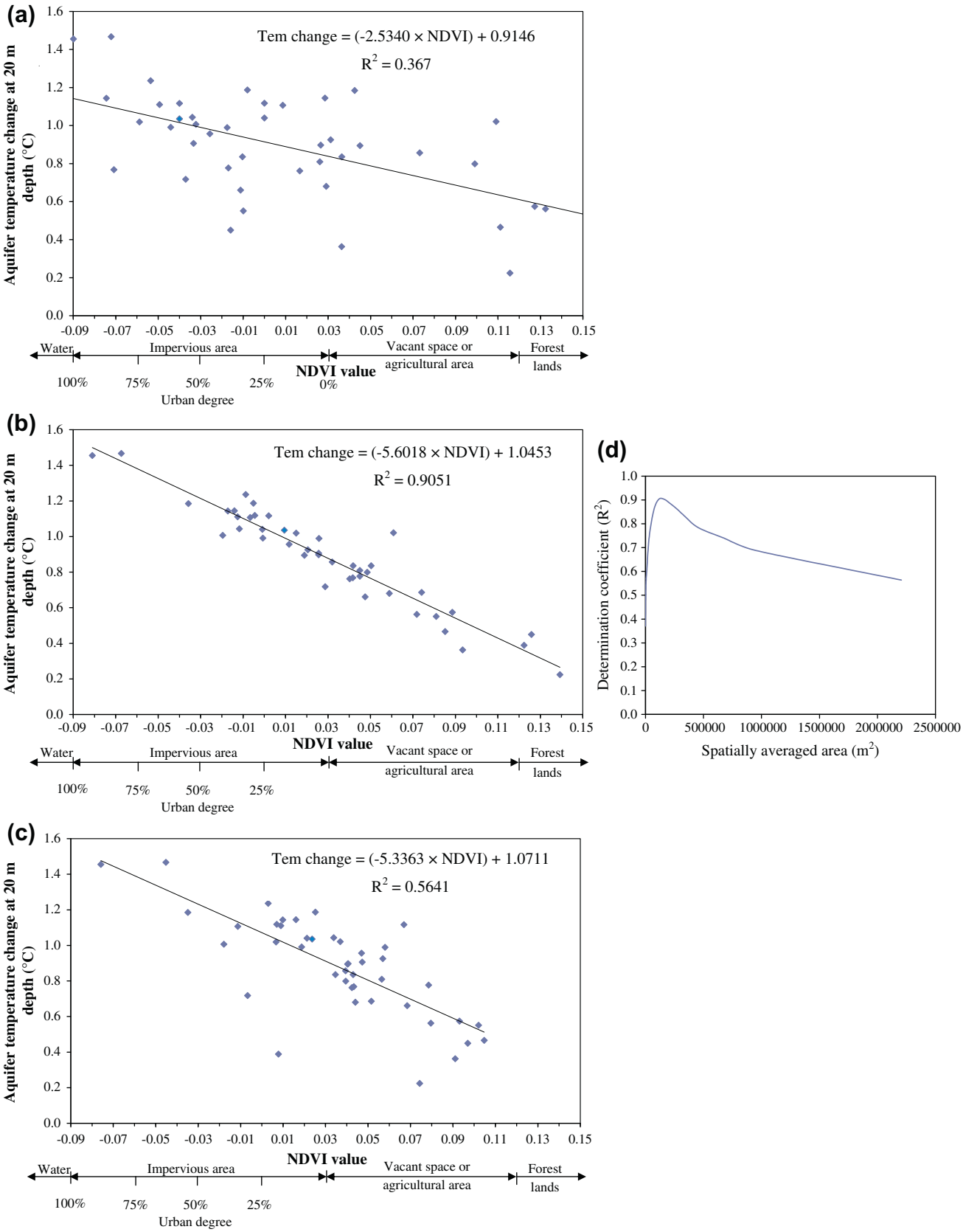

Fig. 7. Relationship between the magnitudes of aquifer temperature changes at a 20-m depth and spatially averaged NDVI values. (a) A single grid box (15×15 m^2), (b) 21 grid boxes on each side ($21 \times 21 \times 15 \times 15$ m^2), (c) 99 grid boxes on each side ($99 \times 99 \times 15 \times 15$ m^2) and (d) change in the determination coefficient for the relationship with a spatially averaged area.

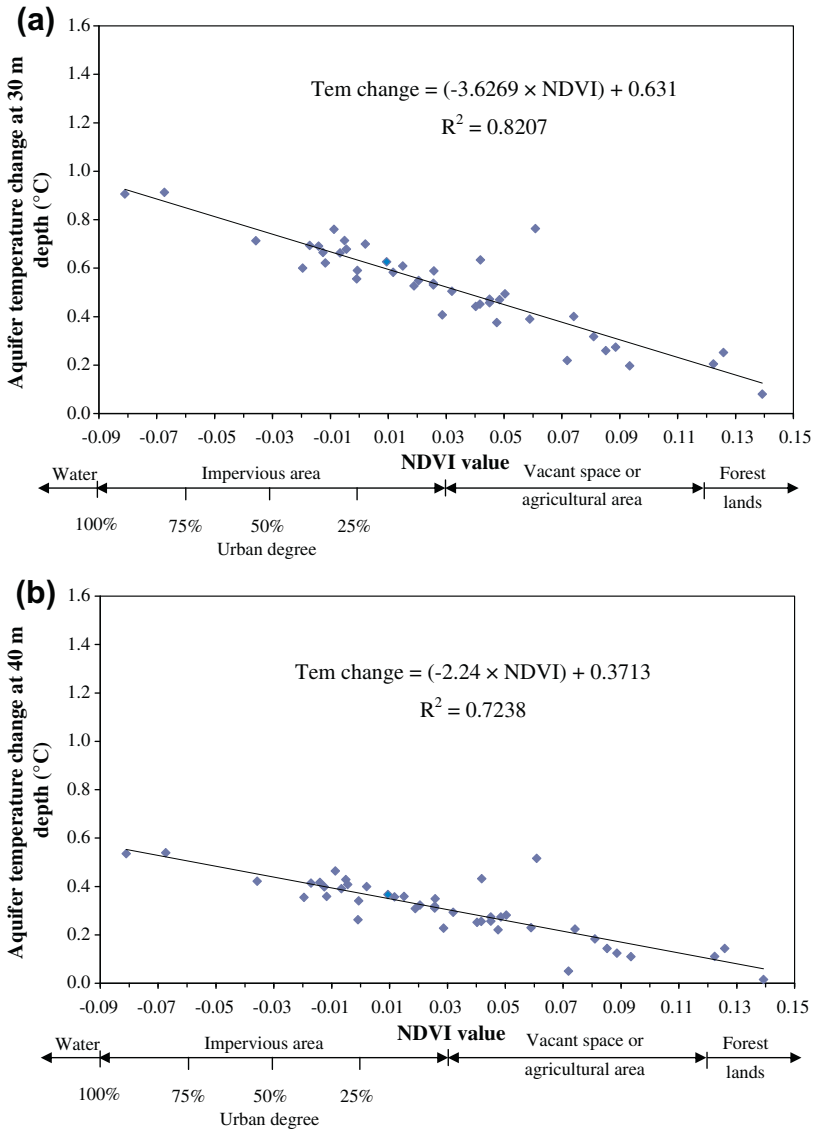

Fig. 8. Relationship between the magnitudes of the aquifer temperature changes and the spatially averaged NDVI values. (a) Temperature change at 30-m and (b) temperature change at 40-m.

temperature–depth profiles collectively used in the Sendai and Chikushi plains. The correlations are strongest at a spatial average of 119,025 m^2 (Fig. 9a), which is slightly higher than the best-fit spatial scale for the Kanto plain (only a 20-m difference). However, the spatially averaged NDVI values for an area of 99,225 m^2 (r = 175 m, the best-fit spatial scale in the Kanto plain) produced a relationship with a 20-m aquifer temperature change and a determination coefficient of 0.81, which closely matches the best-fit determination coefficient for the Chikushi and Sendai plains. The slight difference between two spatial scales can probably be attributed to the spatial resolution of land use data (15 m with pan-sharpening technique). Therefore, the land use characteristics of an area of 80,000–113,500 m^2, which is equal to a circle with a radius of 175 (±15) m, would be appropriate to determine the UHI effect on the subsurface thermal environment.

5. Discussion

By analyzing water levels at different well locations, we confirmed that the horizontal groundwater flow in shallow subsurface layers in the three study areas is not significant. However, Bense and Beltrami (2007) indicated that lateral heat transport due to horizontal groundwater flow becomes important when the flow rate is greater than 10^{-8} m/s. Therefore, when the lateral extent of subsurface heat flow becomes important for practical applications (such as in geothermal energy exploration and in the presence of a significant horizontal groundwater flow), multi-dimensional numerical models will be required to simulate subsurface heat flow.

The analysis performed in this study only incorporates land use characteristics at a local scale. However, subsurface energy change is a cumulative impact attributed to the effects of both urbanization and climate change. Therefore, future studies should apply rigorous methodologies based on the amount of energy increase in subsurface layers to separate the effect of urbanization on aquifer warming from that caused by climate change.

On a more practical view, the operational spatial scale for subsurface warming developed in this study may be used to ensure reliable decision making, and hence is applicable to more general urban planning. This is because UHI studies have traditionally used the ambient air temperatures between urban cities and their rural surroundings (Sakakibara and Owa, 2005; Taniguchi, 2006). With

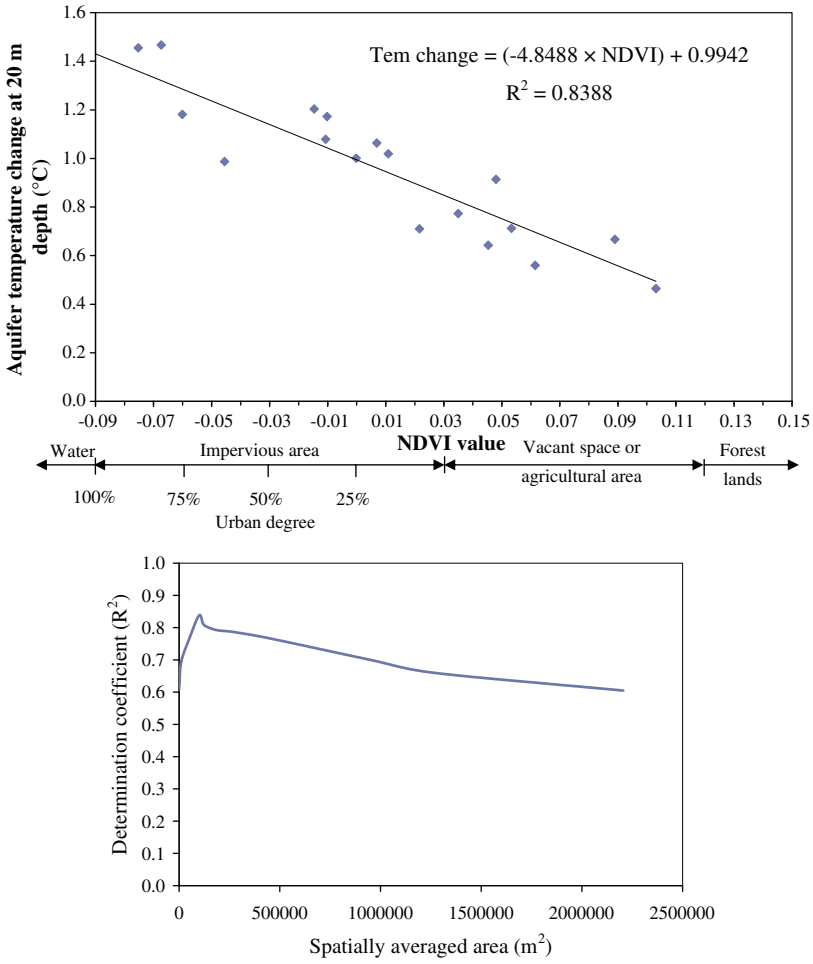

Fig. 9. Relationship between the magnitudes of aquifer temperature changes at a 20-m depth and spatially averaged NDVI values. (a) The best-fit with a spatial scale of 23 grid boxes on each side ($23 \times 23 \times 15 \times 15$ m^2) and (b) the change in the determination coefficient of the relationship with spatially averaged areas.

the advancement of remote sensing technology, satellite observation-derived land surface temperatures are now used to determine the spatial variation of the UHI intensity (Hung et al., 2006; Weng et al., 2004). However, both of these techniques produce a large difference in the magnitude and spatial extent corresponding to diurnal and seasonal variations (Sakakibara and Owa, 2005; Hung et al., 2006). Furthermore, several past studies have estimated the extent of the lateral subsurface temperature distribution attributed to man-made changes. For example, Ferguson and Beltrami (2006) found that the transient temperature anomalies resulting in a deforested area with a width of 500 m might extend 70 m beyond the edge of the deforested area after 100 years. Ferguson and Woodbury (2004) used numerical simulations of heat loss from a temperature-controlled building and found an increase in temperature of 2 °C at a 50-m outward lateral distance from the building after 100 years. However, these studies examined the very specific impacts of a single land use type change with controlled boundary conditions (e.g., a deforestation width of only 500 m or heat loss from a single building). In reality, urban cities are developed in a more complex manner, with various land use type changes at a much broader scale; therefore, the impact on the aquifer thermal regime is more profound and persistent. On the other hand, because of the generally large heat capacity and low thermal diffusivity of the aquifer, the relationship between land use characteristics and aquifer temperature changes obtained in this study may provide a reliable estimation of the spatial extent of the UHI effect on subsurface thermal regimes. Moreover, the results of this study represent the average impact of various land use types over large areas. Thus, even though the estimated lateral extent addressed in this study is slightly larger than the extent proposed by numerical studies, it would be applicable for understanding the UHI effect on subsurface thermal regimes at the scale of a city or an entire plain.

According to the results in the Kanto plain, 0.7 °C reduction in aquifer temperature at a 20-m depth can be achieved by an increased NDVI value of 0.12 (Fig. 7b). Similarly, the verified results in the Sendai and Chikushi plains suggest that 0.6 °C reduction in aquifer temperature at a 20-m depth can be achieved by increasing the NDVI value by the same magnitude (Fig. 9a). The difference of estimated temperature reduction in the two occasions is relatively small (0.1 °C) as compared to the magnitude of temperature change (0.6–0.7 °C). This difference can be attributed to the various observational errors, spatial resolution of land use types (30 m) and in particular to the errors in the classification of the various land uses. Therefore, the uncertainty of our results was interpreted by considering 95% confidence intervals for the coefficient estimated for the independent variable (NDVI value). Table 2 shows a summary of regression statistics corresponding to the relationship between aquifer temperature change and NDVI values. The ranges of aquifer temperature change, estimated for 95% confidence intervals in two occasions, overlap each other, suggesting that 0.5–0.7 °C reduction in aquifer temperature at a 20-m depth can be achieved by increasing NDVI value 0.12.

Table 2
Regression statistics for the relationship between aquifer temperature change and NDVI values.

Study area		Coefficients	Lower 95% CI	Upper 95% CI	Aquifer temperature change at a 20-m depth for 0.12 NDVI change (°C)	
					Lower 95% CI	Upper 95% CI
Kanto	Intercept	1.05	1.01	1.08	−0.60	−0.73
	NDVI variable	−5.60	−6.17	−5.04		
Sendai and Chikushi	Intercept	0.99	0.93	1.05	−0.46	−0.71
	NDVI variable	−4.85	−5.94	−3.76		

6. General implications

In recent studies, the necessity for adaptation measures to cope with urban thermal pollution is increasingly understood. For example, Anderson et al. (2010) examined the thermal impact of removing a culvert and the restoration of groundwater discharge on stream temperature in a highly urban setting in northwestern North Carolina. Rayne et al. (2008) evaluated the effects of riparian forest harvesting on the maximum water temperatures in wetland-sourced headwater streams of British Columbia, Canada. Our study shows that aquifer warming is negatively correlated with the NDVI value, suggesting that land use planning can be used to minimize negative effects on subsurface environment. When the effects of various errors were also considered, a reduction of aquifer temperature in the range of 0.5–0.7 °C at a depth of 20-m can be achieved by increasing the NDVI value by 0.12. Therefore, the developed relationship in this study between the magnitudes of aquifer temperature changes and spatially averaged NDVI values has the potential to be used in urban planning and habitat restoration programs to cope with urban thermal pollution. However, the selected study areas have urbanization histories similar to one another. For example, the surface air temperature in the three regions showed no significant warming trend until the mid-20th century but started to warm rapidly in 1947. Therefore, future studies may need to test the derived spatial extent for regions with different urbanization histories.

7. Conclusions

The heat capacity of the subsurface system is much greater than that of air. Conversely, thermal diffusion is much slower through aquifers than through air. Therefore, strong signatures of ground surface warming are found in shallow subsurface layers. In this study, we matched the subsurface temperature anomalies observed in 43 observation wells in the Kanto plain with grid-averaged NDVI values. The results show that subsurface temperature change is positively correlated with the degree of impervious areas, suggesting that urban development causes subsurface warming (e.g., 0.7 °C warming for a 0.12 NDVI difference at a 20-m depth). The relationship between aquifer temperature changes and grid-averaged NDVI values is strongest for an area covering approximately 175-m with a determination coefficient equal to 0.91 for the Kanto plain. According to results verified with 20 temperature–depth profiles from the Sendai and Chikushi plains, the same relationship was achieved for a 175-m spatial extent with a determination coefficient of 0.81. When the spatial resolution of land use data are concerned, the land use characteristics of an area of 80,000–113,500 m^2, which is equal to a circle with a radius of 175 (±15) m, is suggested as an operational spatial scale to determine the UHI effect on subsurface thermal regimes. As the averaged area is further increased, the relationship between the two variables gradually grows weaker.

Ecologically, aquifer temperature is a key parameter in maintaining desirable thermal conditions for groundwater-dominated ecosystems (e.g., cold groundwater discharge during the summer to streams, wetlands, estuaries and ponds). Conversely, elevated aquifer temperatures of 3–5 °C have been found to be caused by man-made changes in urban environments. These findings imply the importance of evaluating anthropogenic impacts on subsurface environments in urban planning and habitat restoration programs.

Acknowledgements

This work was supported by the JSPS Postdoctoral Fellowship for Foreign Researchers (ID No. P12068) from Japan Society for the Promotion of Science (JSPS) and the Environment Research and Technology Development Fund (S-8) of the Ministry of the Environmental and Grants-in-Aid for Scientific research, Japan. We also thank Hirohisa Matsuure at AIST, Japan for providing the observational data.

References

AIST, 2004. Water Environmental Map No. 1, Sendai Plain. Geological Survey of Japan.
AIST, 2005. Water Environmental Map No. 3, Kanto Plain. Geological Survey of Japan.
AIST, 2008. Water Environmental Map No. 5, Chikushi Plain. Geological Survey of Japan.
Anderson Jr., W.P., Anderson, J.L., Thaxton, C.S., Babyak, C.M., 2010. Changes in stream temperatures in response to restoration of groundwater discharge and solar heating in a culverted, urban stream. J. Hydrol. 393, 309–320.
Arnfield, A.J., 2003. Two decades of urban climate research: a review of turbulence, exchanges of energy and water, and the urban heat island. Int. J. Climatol. 23, 1–26.
Bense, V., Beltrami, H., 2007. Impact of horizontal groundwater flow and localized deforestation on the development of shallow temperature anomalies. J. Geophys. Res. 112, F04015. http://dx.doi.org/10.1029/2006JF000703.
Chen, Z., Stephen, E., Osadetz, K.G., 2002. Predicting average annual groundwater levels from climate variables: an empirical model. J. Hydrol. 260, 102–117.
Drake, J., Bradford, A., Joy, D., 2010. A multi-scale method for identifying groundwater exchanges sustaining critical thermal regimes in streams. Int. J. River Basin Manage. 8, 173–184.
Duque, C., Calvache, M.L., Engesgaard, P., 2010. Investigating river–aquifer relations using water temperature in an anthropized environment (Motril–Salobrena aquifer). J. Hydrol. 381, 121–133.
Epperson, D.L., Davis, J.M., 1995. Estimating the urban bias of surface shelter temperatures using upper-air and satellite data. Part II: Estimation of the urban bias. J. Appl. Meteorol. 34, 358–370.
Essaid, H.I., Zamora, C.M., McCarthy, K.A., Vogel, J.R., Wilson, J.T., 2008. Using heat to characterize streambed water flux variability in four stream reaches. J. Environ. Qual. 37, 1010–1023.
Ferguson, G., Beltrami, H., 2006. Transient lateral heat flow due to land-use changes. Earth Planet. Sci. Lett. 242, 217–222.
Ferguson, G., Woodbury, A.D., 2004. Subsurface heat flow in an urban environment. J. Geophys. Res. 109 (B2), B02402. http://dx.doi.org/10.1029/2003JB002715.
Fujii, H., Inatomi, T., Itoi, R., Uchida, Y., 2007. Development of suitability maps for ground-coupled heat pump systems using groundwater and heat transport models. Geothermics 36, 459–472.
Gallo, K.P., McNab, A.L., Karl, T.R., Brown, J.F., Hood, J.J., Tarpley, J.D., 1993. The use of a vegetation index for assessment of the urban heat island effect. Int. J. Remote Sens. 14, 2223–2230.
Gunawardhana, L.N., Kazama, S., 2009. Tidal effects on aquifer thermal regime: an analytical solution for coastal ecosystem management. J. Hydrol. 377, 377–390.
Gunawardhana, L. N., Kazama, S., 2012. Statistical and numerical analysis of the influence of climate variability on aquifer water levels and groundwater temperatures: The impacts of climate change on aquifer thermal regimes. *Global and Planetary Change,* 86-87, 66–78. http://dx.doi.org/10.1016/j.gloplacha.2012.02.006.
Gunawardhana, L.N., Kazama, S., Kawagoe, S., 2011. Impacts of urbanization and climate change on aquifer thermal regimes. Water Resour. Manage.. http://dx.doi.org/10.1007/s11269-011-9854-6.
Hansen, J., Lebedeff, S., 1987. Global trends of measured surface air temperature. J. Geophys. Res. 92, 13345–13372.

Harris, R.N., Chapman, D.S., 1997. Borehole temperature and a baseline for 20th century global warming estimates. Science 275, 1618–1621.
Healy, R.W., Ronan, A.D., 1996. Documentation of Computer Program VS2DH for Simulation of Energy Transport in Variably Saturated Porous Media – Modification of the US Geological Survey's Computer Program VS2DT, Water-Resources Investigations Report 96–4230, Denver, Colorado.
Huang, S., Pollack, H.N., Shen, P.Y., 2000. Temperature trends over the past five centuries reconstructed from borehole temperatures. Nature 403, 756–758.
Huang, S., Taniguchi, M., Yamano, M., Wang, C., 2009. Detecting urbanization effects on surface and subsurface thermal environment – a case study of Osaka. Sci. Total Environ. 407, 3142–3152.
Hung, T., Uchihama, D., Ochi, S., Yasuoka, Y., 2006. Assessment with satellite data of urban heat island effects in Asian mega cities. Int. J. Appl. Earth Obs. 8, 34–48.
Kataoka, K., Matsumoto, F., Ichinose, T., Taniguchi, M., 2009. Urban warming trends in several large Asian cities over the last 100 years. Sci. Total Environ. 407, 3112–3119.
Majorowicz, J.A., Grasby, S.E., Ferguson, G., Safanda, J., Skinner, W., 2006. Paleoclimatic reconstructions in western Canada from borehole temperature logs: surface air temperature forcing and groundwater flow. Clim. Past 2, 1–10.
Miyakoshi, A., Uchida, Y., 2001. Distribution of surface temperature and groundwater flow systemin the Kanto Plain. Bull. Geol. Sur. Jpn. 52, 253–290 (in Japanese).
Miyakoshi, A., Uchida, Y., Sakura, Y., Hayashi, T., 2003. Distribution of subsurface temperature in the Kanto Plain, Japan; estimation of regional groundwater flow system and surface warming. Phys. Chem. Earth 28, 467–475.
Oke, T.R., 1973. City size and the urban heat island. Atmos. Environ. 7, 769–779.
Pollack, H.N., Huang, S., Shen, P.Y., 1998. Climate change record in subsurface temperatures: a global perspective. Science 282, 279.
Rayne, S., Henderson, G., Gill, P., Forest, K., 2008. Riparian forest harvesting effects on maximum water temperatures in wetland-sourced headwater streams from the Nicola River Watershed, British Columbia, Canada. Water Resour. Manage. 22, 565–578.
Sakakibara, Y., Owa, K., 2005. Urban–rural temperature differences in coastal cities: influence of rural sites. Int. J. Climatol. 25, 811–820.
Su, G.W., Jasperse, J., Seymour, D., Constantz, J., 2004. Estimation of hydraulic conductivity in an alluvial system using temperatures. Ground Water 42, 890–901.
Suzuki, H., 1996. Geology of Koto deep borehole observatory and geological structure beneath the metropolitan area, Japan. Natl. Res. Inst. Earth Sci. Disaster Prev. Jpn. 56, 77–123.
Taniguchi, M., 2006. Anthropogenic effects on subsurface temperature in Bangkok. Clim. Past Discuss. 2, 831–846.
Taniguchi, M., Shimada, J., Tanaka, T., Kayane, I., Sakura, Y., Shimano, Y., Siakwan, S.D., Kawashima, S., 1999. Disturbances of temperature–depth profiles due to surface climate-change and subsurface water flow: (1) an effect of linear increase in surface temperature caused by global warming and urbanization in the Tokyo metropolitan area, Japan. Water Resour. Res. 35, 1507–1517.
Uchida, Y., Hayashi, T., 2005. Effects of hydrogeological and climate change on the subsurface thermal regime in the Sendai Plain. Phys. Earth Planet. In. 152, 292–304.
Weng, Q., Lu, D., Schubring, J., 2004. Estimation of land-surface temperature–vegetation abundance relationship for urban heat island studies. Remote Sens. Environ. 89, 467–483.
Ziagos, J.P., Blackwell, D.D., 1986. A model for the transient temperature effects of horizontal fluid flow in geothermal systems. J. Volcanol. Geoth. Res. 27, 371–397.